Supplementary Information

Polaritonic Fourier Crystal

Sergey G. Menabde,[1,†] Yongjun Lim,[2,†] Kirill Voronin,[3,†] Jacob T. Heiden,[1] Alexey Y. Nikitin,[3,4,*] Seungwoo Lee,[2,5,6,**] and Min Seok Jang[1,***]

[1]School of Electrical Engineering, Korea Advanced Institute of Science and Technology, Daejeon 34141, Korea

[2]Department of Biomicrosystem Technology, Korea University, Seoul 02841, Korea

[3]Donostia International Physics Center (DIPC), Donostia-San Sebastián 20018, Spain

[4]IKERBASQUE, Basque Foundation for Science, Bilbao 48013, Spain

[5]Department of Integrative Energy Engineering, KU-KIST Graduate School of Converging Science and Technology, and KU Photonics Center, Korea University, Seoul 02841, Korea

[6]Center for Opto-Electronic Materials and Devices, Post-Silicon Semiconductor Institute, Korea Institute of Science and Technology (KIST), Seoul 02792, Korea

[†] These authors contributed equally to this work.

[*]alexey@dipc.org

[**]seungwoo@korea.ac.kr

[***]jang.minseok@kaist.ac.kr

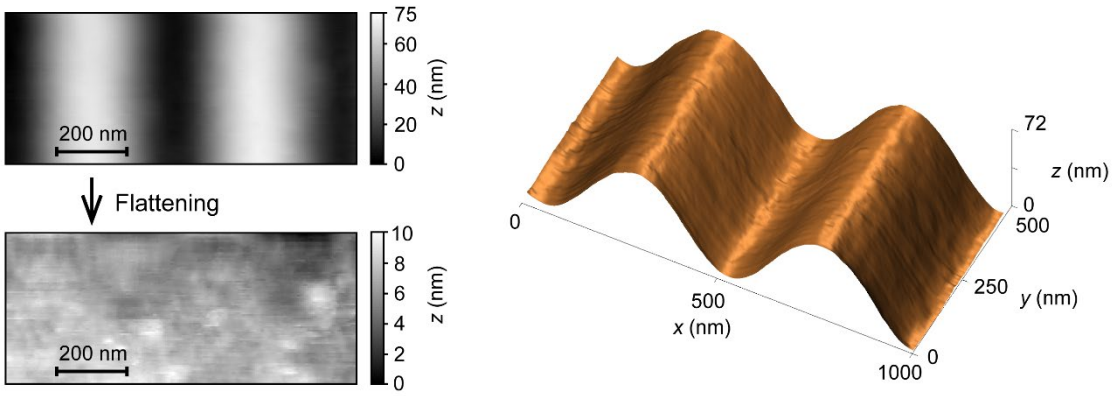

Figure S1. High-resolution AFM scan of the gold-covered Fourier surface next to the hBN flake shown in Figure 2 in the main text. To measure the RMS roughness, the original AFM scan (top left) was rotated by 90 degrees and flattened by the line leveling algorithm, and rotated back to the same orientation (bottom left). Then, roughness of the flattened AFM data was measured, indicating the RMS value of 1.4 nm. Right: 3D render of the AFM data; note the exaggerated scale in the *z*-direction.

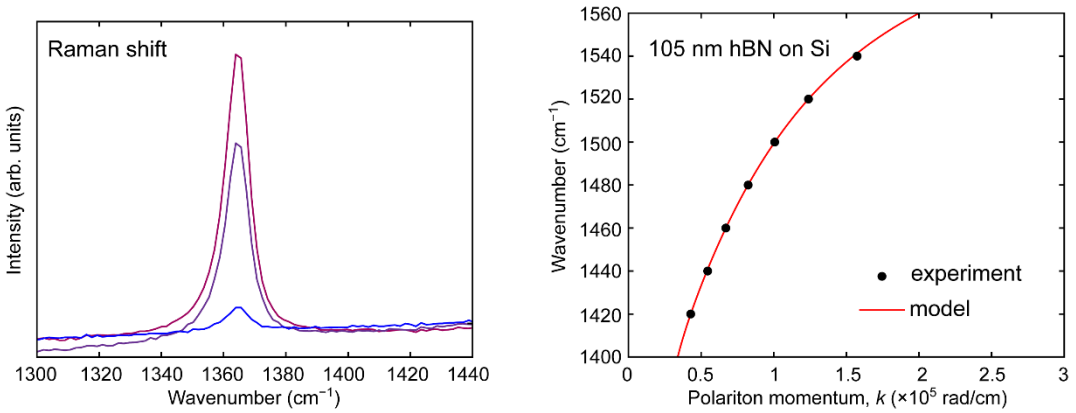

Figure S2. Left: Raman spectra of three hBN flakes of different thickness, all providing the TO phonon frequency of 1364.3 cm^{-1}. Right: HPhP dispersion in 105 nm-tick hBN on Si substrate measured by s-SNOM (data points). Both Raman and near-field data was used to obtain the parameters of the hBN dielectric function provided in Table S1 below. The ~2 nm-thick native SiO_2 layer is confirmed to cause insignificant deviation of the HPhP dispersion and is not accounted for during the fitting procedure.

	ω_{LO}, cm^{-1}	ω_{TO}, cm^{-1}	Γ, cm^{-1}	ε_∞
In-plane	1619.8	1364.3	5.3	5.22
Out-of-plane	820.2	761.0	3	2.25

Table S1. Parameters of hBN dielectric function used for modeling. Parameters fitted from the Raman spectroscopy (Figure S1, left) are shown in blue, and those fitted from near-field dispersion measurements (Figure S1, tight) are shown in red. The damping parameter is adopted from the literature for the naturally abundant hBN.

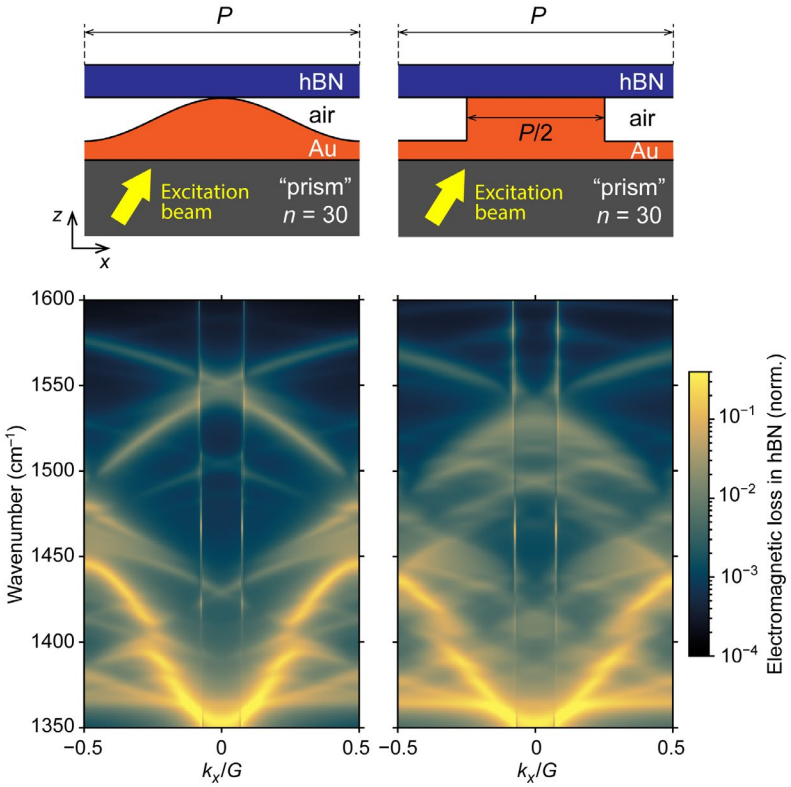

Figure S3. Full-wave simulation model (top row) to calculate the band structure in the Fourier crystal (left) and in the grating with sharp edges (right). Both structures have the same maximal air gap size and the period P. The gold-hBN contact length in the grating is set to $P/2$. Both band structures are calculated by full-wave numerical simulations in 2D domain with periodic boundary conditions on both sides of the unit cell. Color map shows the electromagnetic loss density in the hBN slab as a function of the excitation frequency and x-component of the wavevector of the excitation beam. The simulated excitation scheme mimics the Otto configuration where the TM-polarized plane wave illuminates the structure from the side of the substrate, which is typically a coupling prism made of a high-index material. In the simulations, the excitation wave is launched by a periodic port immersed in a fictitious high-index "prism" with $n = 30$. Such a high index is required to sweep through the necessary k_x values with relatively small incidence angles < 25°. This provides a relatively uniform excitation efficiency due to the small variation of the reflection coefficient of the interface.

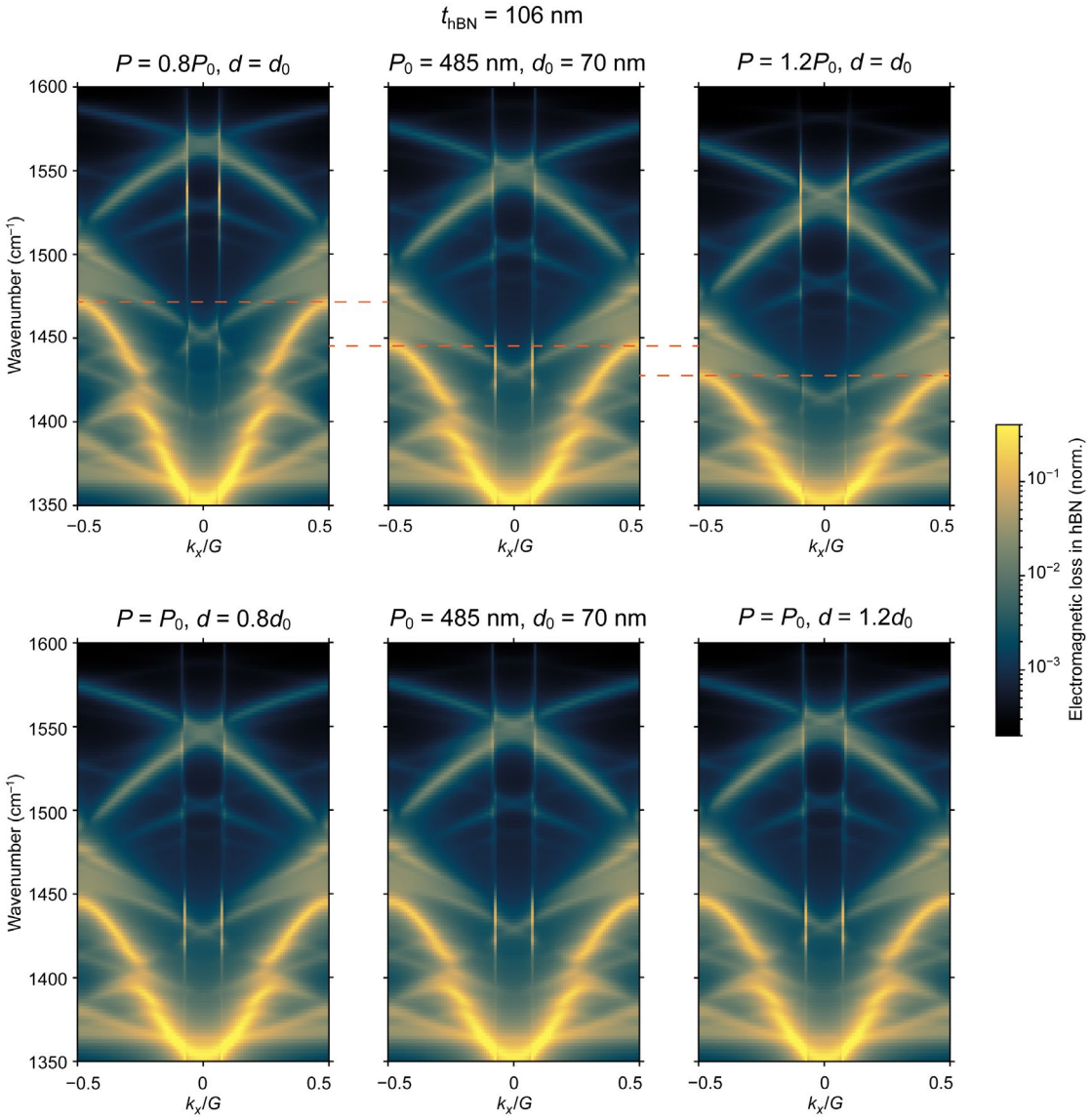

Figure S4. Band structure of HPhP in the Fourier crystal with 106 nm-thick hBN and varying parameters of the corrugated surface, calculated by full-wave FEM simulations. Top row: results of variation of corrugation period P by ±20% compared to the experimentally investigated structure with P = 485 nm and d = 70 nm (middle panel). Bottom row: results of variation of corrugation depth d by ±20% compared to the experimentally investigated structure (middle panel). Band diagrams are obtained by mapping the electromagnetic loss density in hBN slab under the different excitation frequencies and momenta, as explained in the caption of Fig. S3.

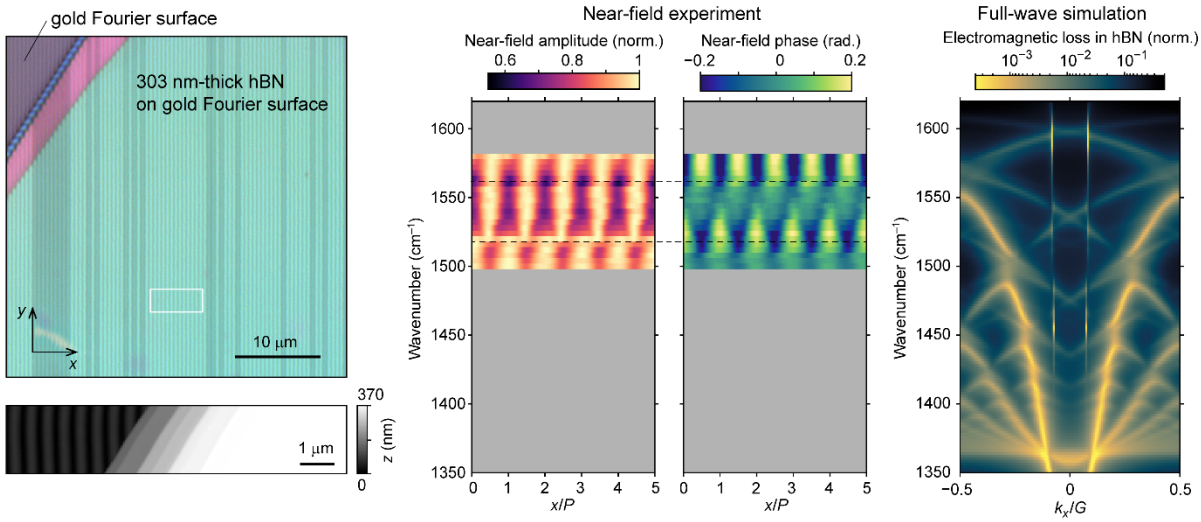

Figure S5. Left: optical image of the 303 nm-thick hBN flake deposited on the gilded azopolymer Fourier surface, and AFM profile across the hBN edge (outside the imaged area). Middle: near-field amplitude and phase maps measured far from the hBN edges (around the area marked by the white rectangle on the optical image). Right: band structure of Bloch modes in the FC, obtained by full-wave numerical simulations in 2D domain as discussed in Fig. S3.

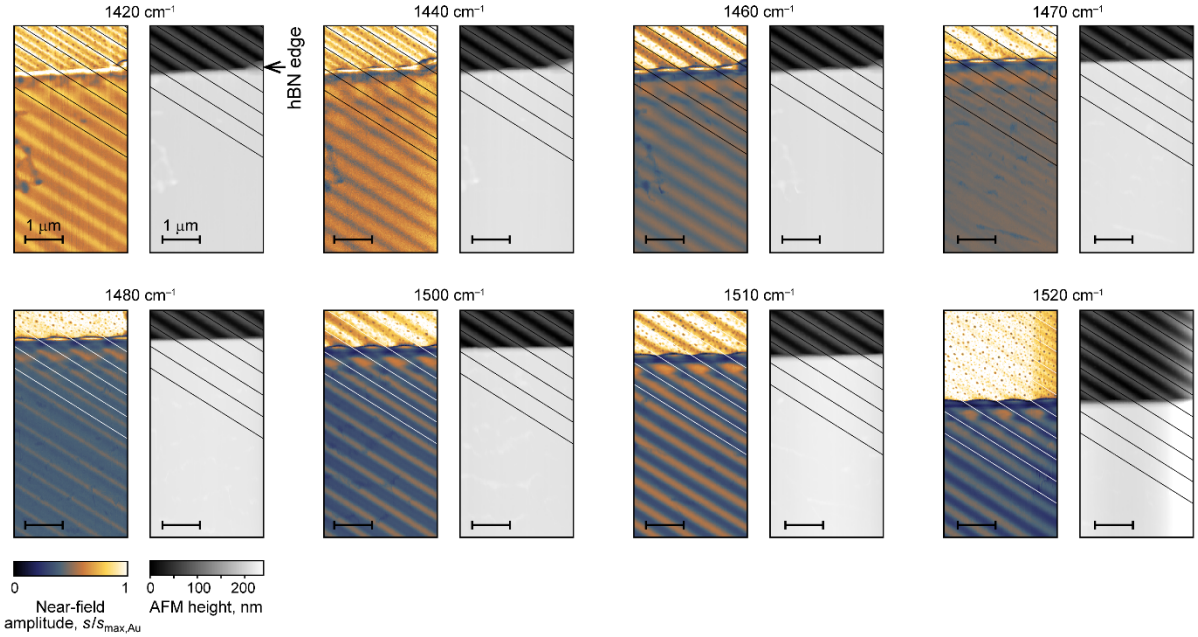

Figure S6. Near-field amplitude images and corresponding AFM profiles of the hBN edge measured by s-SNOM at different frequencies. Near-field is normalized by the maximum over the gold surface, showing the varying amplitude above the Fourier crystal depending on frequency. The generally stronger signal over hBN at lower frequencies can be explained by the more negative in-plane permittivity of hBN. Straight lines indicate the maxima of the gold surface where it is in contact with the hBN slab. Note that the near-field amplitude peaks become misaligned with the surface maxima by $P/2$ as soon as the excitation frequency exceeds the expected upper limit of the M0 bandgap at 1470 cm^{-1}.

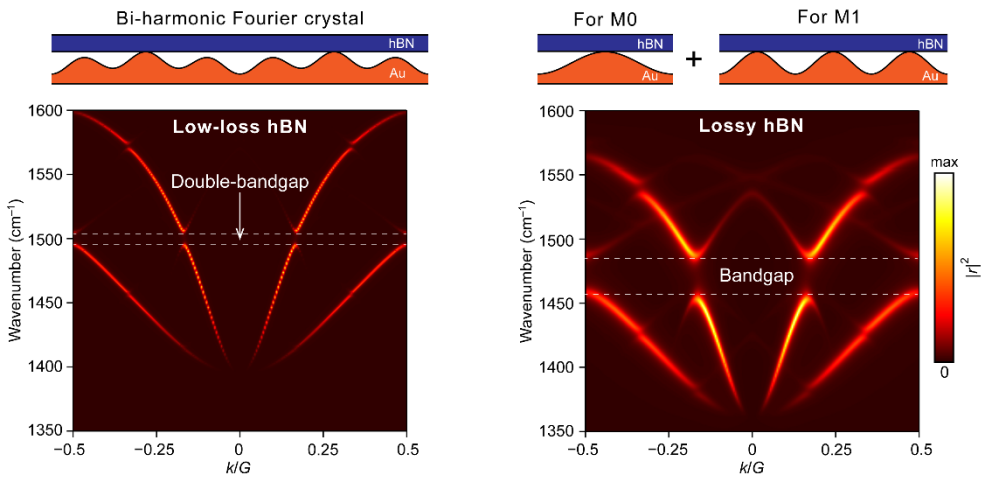

Figure S7. Left: a double-bandgap opening for M0 and M1 phonon-polariton modes in a bi-harmonic Fourier crystal with 106 nm-thick low-loss isotopically pure hBN. Surface profile is exaggerated. Right: A sum of the two band diagrams calculated independently for M0 and M1 modes in the respective structures with lossy (naturally abundant) hBN. Surface profiles are not in scale.